21

Carbon Nanotubes Addition Effects on MgB_2 Superconducting Properties

Adriana Serquis[1], Gabriela Pasquini[2] and Leonardo Civale[3]
[1]*Instituto Balseiro-UNCuyo, Centro Atómico Bariloche – CNEA, CONICET*
[2]*Dept. de Física – FCEyN - Universidad de Buenos Aires, IFIBA - CONICET*
[3]*MPA-STC, Los Alamos National Laboratory*
[1,2]*Argentina*
[3]*USA*

1. Introduction

Since the discovery of superconductivity at 39 K in MgB_2 (Nagamatsu et al., 2001), considerable progress has been made in the understanding of the fundamental properties and the development of commercial applications of this material.

The strong potential for technological uses of MgB_2 is due to a unique combination of characteristics, such as a high transition temperature T_c ~ 39K, chemical simplicity, lightweight and low cost of the raw materials (Buzea et al., 2001). In addition, the absence of weak-link behavior at grain boundaries in polycrystalline samples (Larbalestier et al., 2001) allows the use of simple Powder in Tube (PIT) methods to fabricate wires and tapes (Flükiger et al., 2003). One of the most important issues for MgB_2 magnet applications is the simultaneous enhancement of its critical current density (J_c) and the upper critical field (H_{c2}). Thus, on one hand, the pinning force may be improved by the incorporation of defects (nano particle doping, chemical substitutions, etc.). On the other hand, the doping level affects the intraband scattering coefficients and the diffusivity of the two bands of this peculiar superconductor, and these changes may cause a significant H_{c2} variation. Carbon or C-compounds additions have been very successful to improve J_c and/or H_{c2}, and the effects of carbon doping on superconductivity in MgB_2 has been extensively studied. The J_c-H performance can be greatly improved by adding different carbon sources, such as carbon doped MgB_2 filaments (Wilke et al., 2004, 2005a), nanocarbon (Soltanian et al., 2003; Ma et al., 2006; Yeoh et al., 2006; Häβler et al., 2008), amorphous carbon (Senkowicz et al., 2005), diamond (Cheng et al., 2003), B_4C (Wilke et al., 2005b; Ueda et al., 2005; Yamamoto et al., 2005a, 2005b), carbon nanohorn (Ban et al., 2005) and, particularly, carbon nanotubes (Dou et al., 2003; Yeoh et al., 2004, 2005, 2006; Serquis et al., 2007; Serrano et al., 2008, 2009); Shekhar, 2007; Vajpayee et al., 2010; etc).

In this chapter we present a review of recent developments in the study of the effect of carbon nanotubes (CNT) on the superconducting properties of MgB_2 bulk and wire samples, based on the known literature data and our own results.

It is well known that pinning of vortex lines to defects in superconductors plays an extremely important role in determining their properties. CNT inclusions, with diameters close to the MgB_2 coherence length ($\xi_{ab}(0)$ ~ 3.7-12nm; $\xi_c(0)$ ~ 1.6-3.6 nm, depending on the

doping level, as discussed below in section 2.1.2) (Buzea et al., 2001) may be very good candidates for vortex pinning if they do not completely dissolve in the matrix but remain as tubes acting as columnar defects. Therefore, the presence of CNT may result in a critical current density improvement under applied fields that will depend on the synthesis parameters. Besides, theoretical models predict that the presence of two superconducting gaps could allow tuning of different upper critical fields by controlling diverse defect sublattices relative to orthogonal hybrid bands (Golubov et al., 2002; Gurevich , 2003). These models predict a significant H_{c2} enhancement in the dirty limit and an anomalous $H_{c2}(T)$ upward curvature. Several reports indicate that H_{c2} can be significantly increased by introducing disorder through oxygen alloying, carbon doping or He-ion irradiation (Brinkmann et al., 2002; Gurevich et al., 2004; Putti et al., 2004; Braccini et al., 2005). Thus, it is important to analyze the effect of carbon-doping through CNT or other C-sources to the $H_{c2}(T)$ in bulk MgB_2 samples, where extrapolated values of $H_{c2}(0)$ between 29 and 44 T have been reported (Wilke et al., 2004; Senkowicz et al., 2005; Serquis et al., 2007; Serrano et al., 2008).

In section 2 of this work, we describe the influence of C-incorporation into the MgB_2 structure by using different CNT type over the microstructural and superconducting properties (critical current density, critical fields and critical temperature). In particular. we present the influence of synthesis parameters in the superconductivity of bulk samples prepared with single-walled (SW), double-walled (DW) and multi-walled (MW). In the first subsection, we compare the evolution of T_c, and the lattice parameters with the amount of CNT, analyzing if C is replacing B in the $Mg(B_{1-x}C_x)_2$ structure or remains as CNT in each case. In the following subsections, we present a review of J_c determined by magnetization, and H_{c2}(T) by transport measurements, which may require measurements performed using high fields (i.e. 50 T) pulsed magnets. In the last subsection, we also present an analysis of the distinctive effect of C addition in samples with optimum contents of single-walled and double-walled carbon nanotubes SiC, that simultaneously increase J_c and H_{c2}.

In section 3, we offer a review of the use of CNT in the production of PIT MgB_2 wires and tapes required for applications. The fabrication and processing conditions strongly affect microstructures and current carrying capability of PIT conductors, making the question of grain connectivity more relevant. The standard and low-cost fabrication PIT method involves filling a metallic tube with superconducting powder (ex-situ) or precursors (in-situ) and drawing it into a wire and/or rolling into a tape (Flükiger et al., 2003). We show the results obtained in MgB_2 wires and tapes prepared by PIT using different kind of CNT and treated at different temperatures between 600 and 900 °C, using several sheath materials (e.g. iron, stainless steel, Fe/Nb, etc), to establish a relationship among annealing conditions, modifications in the microstructure, and changes in J_c.

In Section 4 we go deeper in the role of doping by studying the magnetic relaxation of MgB_2 with and without DWCNT bulk samples. In the first subsection, we introduce the main equations contained in a very recent work (Pasquini et al., 2011) necessary to investigate the current decay, that relates parameters such as the magnetic field B, the magnetization m, current density J flowing in the sample, and the activation barrier $U(J,T,B)$ that governs the creep of vortices. In the rest of this section we present the experimental relaxation rates (measured using a DC magnetization technique), and the general behaviour is described and analyzed under the Anderson-Kim frame model (Anderson, 1964). The pinning energies U_c, true critical current densities J_{c0}, and correlation volumes V_c are estimated and compared.

Finally, we summarize the main conclusions in section 6.

2. Effect of different kind of CNT addition to superconducting properties of MgB_2 bulk samples

There are many reports in the literature that study the effect of CNT on the superconducting properties of MgB_2. However, many of them mentioned the effect of CNT-doping without clarifying the meaning of this word. *Doping* is generally the practice of adding impurities to something, but it specifically means the replacement of one element within the same crystalline structure, creating a substitutional point defect. In the case of CNT additions to MgB_2 it is possible that part of the carbon replaces boron giving place to the compound $Mg(B_{1-x}C_x)_2$. As a consequence, in many works, the nominal amount of CNTs added during the synthesis is calculated as the stoichiometric amount according to this formula or, in other cases as some extra %at or %wt of carbon added to MgB_2. In the later case, if part of carbon replaces boron, some extra magnesium should be added that may also evaporate or form MgO during the synthesis process. In this chapter, unless it is specified, we will use "x" as the nominal amount of carbon added according to $Mg(B_{1-x}C_x)_2$, and the term "doping" when carbon is actually replacing boron.

2.1 Carbon doping and critical temperature (T_c)

Several systematic carbon doping studies of $Mg(B_{1-x}C_x)_2$ have been performed in single crystals (Lee et al., 2003; Kazakov et al., 2005), polycrystalline wires fabricated by chemical vapor deposition (CVD) (Wilke et al., 2004, 2005a), and B_4C-doped (Avdeev et al., 2003; Wilke et al., 2005b). All these studies indicate a monotonic decrease of T_c and the lattice parameter a for increasing x, while the lattice parameter c remains constant.

For single crystals, the solubility limit of C in MgB_2 was estimated to be about 15 ± 1%, which is substantially larger than that reported for the polycrystalline samples. A dramatic decrease in T_c was also observed with C-substitution, followed by complete suppression of superconductivity for x>0.125. This solubility limit is usually not reached in bulk samples. A comparison of the critical temperature as a function of the nominal C-content for different carbon sources is displayed in Figure 1.

The reduction in T_c resulting from C addition using CNT sources is much lower than in the previous cases, suggesting that C substitution is lower than the concentration given by $Mg(B_{1-x}C_x)_2$. The T_c decrease is even lower when using SWCNT as a source of carbon indicating a very low doping level.

As an example, it is possible to calculate the actual C content substituting B into the MgB_2 structure, using the lattice parameters obtained from XRD: the shift in the a-axis lattice parameter can be used as a calibration for the actual amount of C (x) in the $Mg(B_{1-x}C_x)_2$ structure in comparison with the fitting of neutron diffraction data (Avdeev et al., 2003) or single crystal data (Kazakov et al., 2005). The dependence of a-axis lattice parameter as a function of the nominal DWCNT %at content is plotted in Figure 2. The corrected x values obtained were used to plot the same data as open squares in Figure 1, indicating that not all C is incorporated into the MgB_2 structure. A similar behavior is observed for all CNT samples, indicating that actual C-substitution tends to saturate for nominal CNT contents larger than 10%at. The actual C-doping varies according to the CNT type, synthesis temperature or other synthesis parameters (i.e. pressure or magnetic field). This C-substitution level determines not only the T_c but other superconducting properties such as H_{c2}, as will be described in section 2.2. Nevertheless, we will continue using the nominal content as the parameter to describe most effects to make it easier the comparison with other author's results.

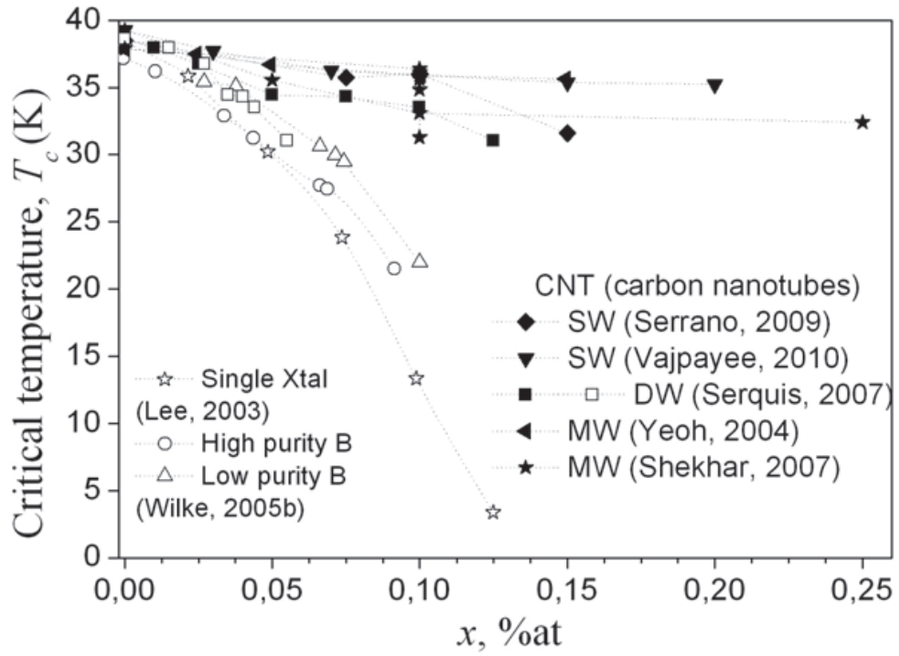

Fig. 1. Critical temperature as a function of the nominal C-content using different carbon sources.

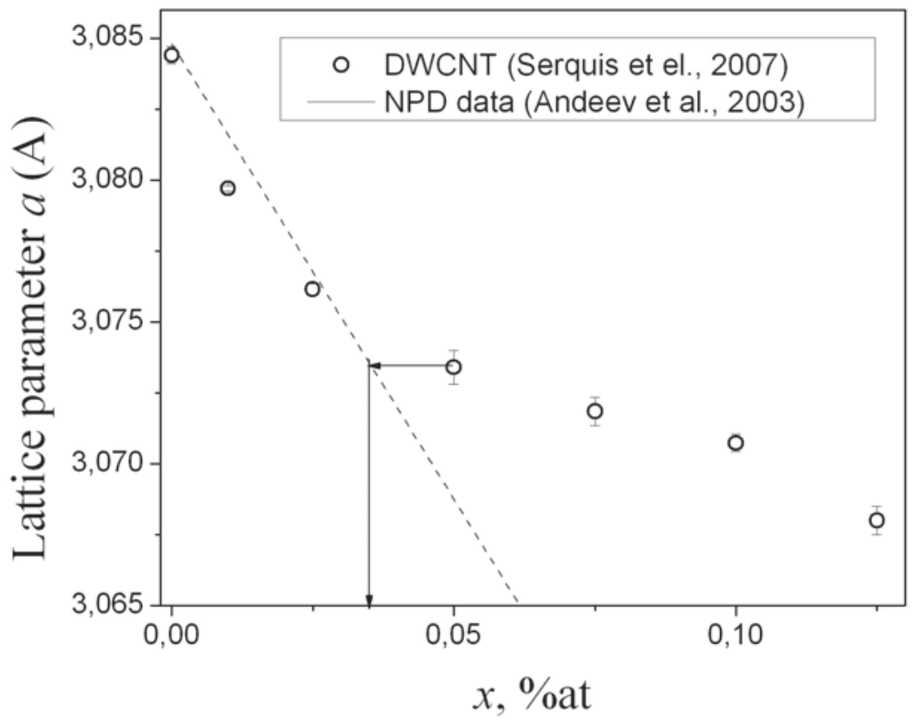

Fig. 2. Lattice parameter *a* as a function of the nominal C-content for DWCNT samples compared with others with full carbon substitution, measured by neutron diffraction.

It is important to mention that not only the nominal carbon content x but also other synthesis parameters affect the superconducting properties like T_c due to the amount of C substituting B in the structure. All parameters studied up to now are listed at the beginning of next section.

2.2 Simultaneous enhancement of critical currents and fields

2.2.1 Critical currents (J_c)

Since the first work devoted to the study of the effect of the addition of CNT on the critical current density of MgB_2 (Dou et al., 2003), several parameters have been studied:

- the amount of "x" for a particular CNT type : MWCNT (Dou et al., 2003; Shekhar, 2007), DWCNT (Serquis et al., 2007), SWCNT (Serrano et al., 2009 ; Vajpayee et al., 2010)
- the effect of CNT type (Serrano et al., 2008) and size (Yeoh et al., 2005, 2006)
- the effect of sintering conditions such as temperature (Yeoh et al., 2004), pressure (Yuan et al., 2005), ultrasonication of precursors (Yeoh et al., 2006) or the application of magnetic field during sintering (Li et al., 2007)

Most researchers performed magnetization loops measurements to determine $J_c(H)$ in bulk samples using the Bean critical state model (Bean, 1962) assuming full penetrated samples for a long parallelepiped:

$$J_c(H)[A/cm^2] = \frac{20 \times \Delta M(H)[emu/cm^3]}{(a - \frac{a^2}{3b})[cm]} \quad (1)$$

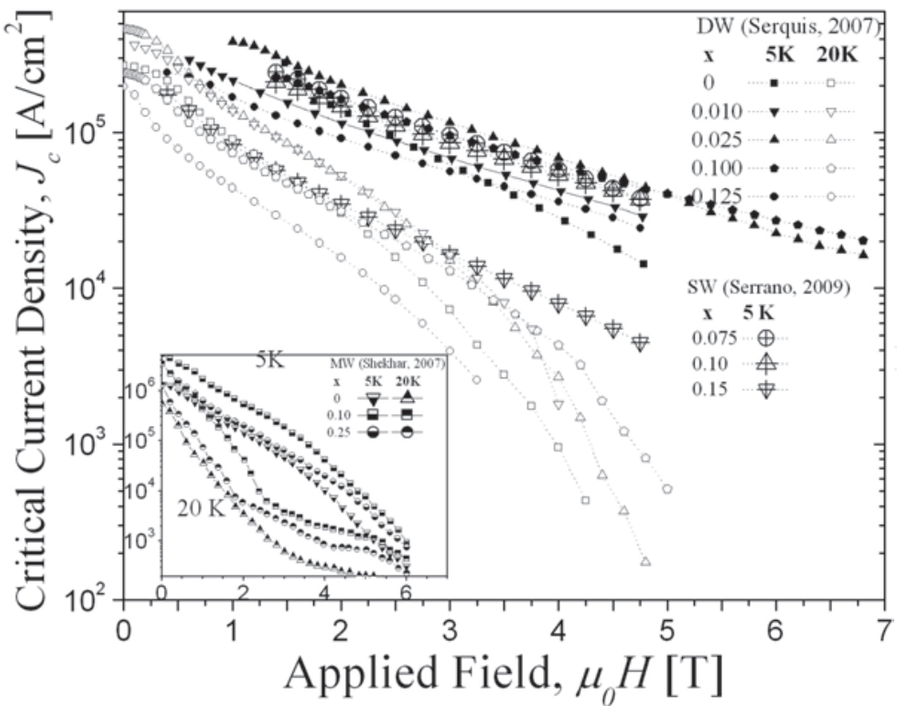

Fig. 3. J_c field dependence determined by magnetization for samples with different amount of SW, DW and MW CNT at 5K and 20 K. Data from MWCNT (Shekhar et al., 2007), DWCNT (Serquis et al., 2007) and SWCNT (Serrano et al., 2009)

where *a* and *b* are the lengths of the parallelepiped edges perpendicular to the magnetic field and ΔM is the width of the magnetization characteristic at the applied magnetic field *H*.
Figure 3 shows the dependence of J_c with the applied magnetic field at 5 and 20 K for samples prepared with different amount of single (SW) (Serrano et al., 2009), double (DW) (Serquis et al., 2007) and multi-walled (MW) (Shekhar et al., 2007) CNT (see inset for the later case). Some flux jumps were frequently reported at 5 K in regions up to 2 T, and these data were not included in the corresponding figures. It can be observed that in all cases the addition of CNT progressively improves the overall $J_c(H)$ performance, reaching an optimum for the x=0.10 sample, where J_c is higher than for any other composition in all the reported temperatures and fields. When the amount of added CNT is over 10%at the performance deteriorates. However, many other authors also reported that the optimum addition is around 10%at, although in some cases the critical current densities are not higher than for other compositions in the whole range of temperatures or applied fields.

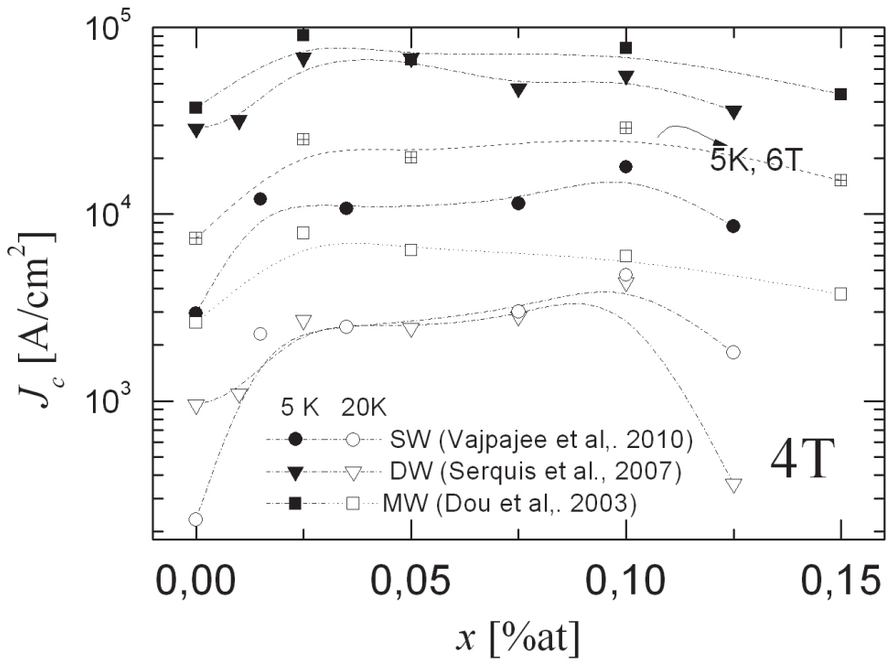

Fig. 4. Critical current densities at 4 T as determined by magnetization as a function of the amount of SW (circles), DW (triangles) and MW (squares) CNT added to MgB_2 at 5K (full symbols) and 20 K (open symbols). Data from MWCNT (Dou et al., 2003), DWCNT (Serquis et al., 2007) and SWCNT (Vajpayee et al., 2010)

Figure 4 displays the dependence of J_c with different amount of MWCNT (Dou et al., 2003), DWCNT (Serquis et al., 2007) and SWCNT (Vajpayee et al., 2010) added to MgB_2 samples under an applied field of 4 T and temperatures of 5 and 20 K. It is interesting to note that the critical current densities are very similar between x = 0,025 and x = 0,10 for each type of sample, but the J_c improvement tends to be more notorious for x = 0,10 at higher temperatures and fields. The best composition for a certain field and temperature may also change with the sintering temperature. Samples included in Figure 4 were prepared at 800, 900 and 850°C for MW, DW and SW, respectively. A study about the dependence with

sintering temperature (Ts) in MgB_2 samples with MW CNT (Yeoh et al., 2004) indicated that when the Ts is 900°C or higher, the nanotubes tend to dissolve and are incorporated into the MgB_2 matrix, decreasing T_c but increasing the irreversibility field (H_{irr}). This effect will be discussed in the next subsection, since it is correlated with the H_{c2} improvement. Therefore, the larger the amount of C-doping the smaller is the $J_c(H)$ slope improving the performance at higher fields. On the contrary, the J_c decrease for x > 0,10 may be due to both an even larger decrease in T_c and a probable deterioration of interconnectivity between grains. This deterioration of grain connectivity was denoted by a large normal resistivity value (i.e. ρ(40K) ~ 200 μΩcm) for the DW sample with x = 0,125.
Figure 5 shows the dependence of J_c with the applied magnetic field of samples prepared with the same amount of single (SW), double (DW) and multi-walled (MW) CNT.

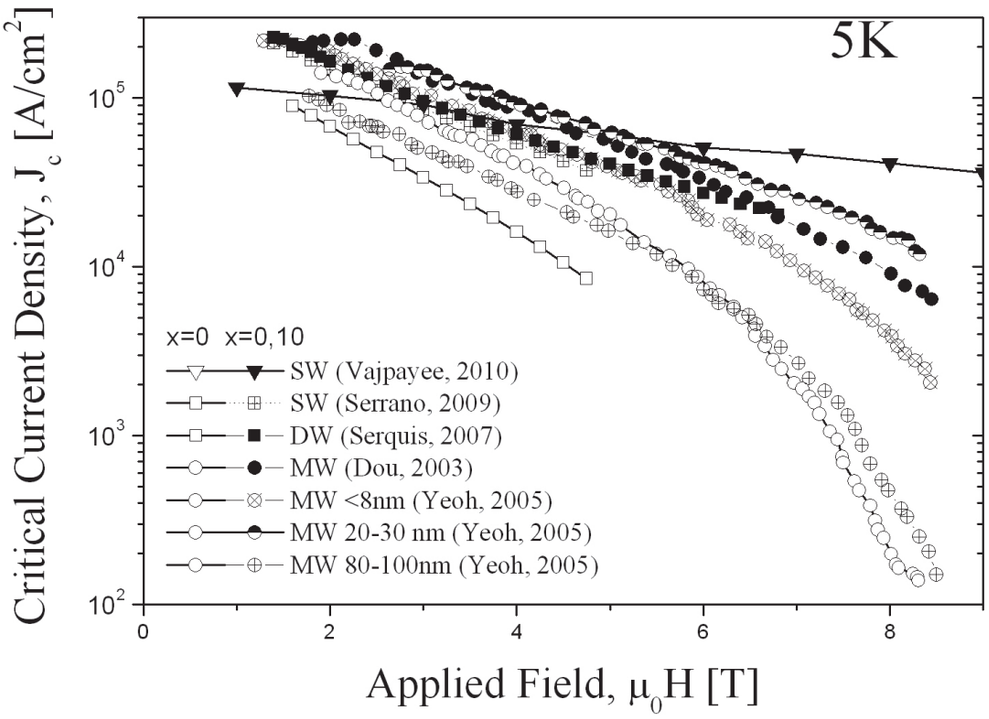

Fig. 5. J_c field dependence determined by magnetization at 5K and 20 K for samples with the same nominal composition (x=0,10) but different CNT types (SW, DW and MW of different sizes). The corresponding pure samples (x = 0) are included as references (open symbols)

For comparing the absolute values it is important to take into account the pure MgB2 sample used as reference since this can be a good parameter to check the influence of variables other than composition, such as connectivity, that may result from the sintering process. Consequently, the best performances (i.e. Jc values and Jc(H) dependences) are obtained for MW (diameter 20-30 nm) (Yeoh et al., 2005) and DW (diameter 1.3–5 nm) (Serquis et al., 2007). These two samples (both heat treated in flowing high purity Ar at 900 for 30 minutes) presented the largest C-doping (smallest *a* lattice parameter) and Yeoh et al. suggested that it is not the diameter but the MWCNT length the responsible for allowing a more homogeneous C-incorporation by avoiding the nanotubes agglomeration. This explanation may not apply to DW CNTs, which have a length ≤ 50 μm. However, it is highly

probable that synthesis parameters that promote a more homogeneous CNT distribution and improve connectivity (avoiding agglomerates at grain boundaries) are the key for Jc performance.

2.2.2 Upper critical fields (H_{c2})

The $H_{c2}(T)$ dependences are usually determined from four probe transport measurements. Since the involved fields are frequently very high for standard laboratory test equipments, several groups performed measurements at large High Magnetic Field facilities. As an example, measurements of DW and SW CNT samples were performed in the mid-pulse magnet of NHMFL-LANL, capable of generating an asymmetric field pulse up to 50 T. Figure 6 exhibits the temperature dependences of H_{c2} and H_{irr}, defined as the onset (extrapolation of the maximum slope up to the normal state resistivity) and the beginning of the dissipation, respectively, of the R versus H data for samples with several DWCNT contents, at temperatures between 1.4 and 34 K. The criteria to define H_{c2} and H_{irr} are exemplified in the inset of figure 6.

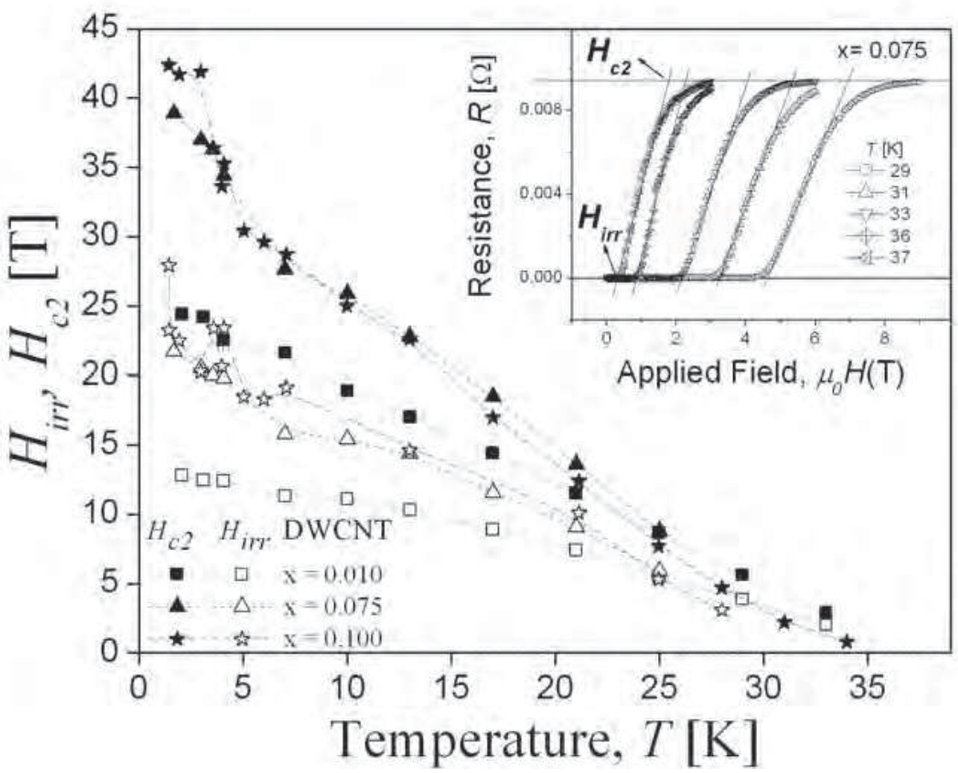

Fig. 6. Transport measurements of the upper critical field (H_{c2}) and the beginning of the dissipation (H_{irr}) as a function of temperature for samples with DWCNT contents of 0.01, 0.075 and 0.10. The inset shows some of $R(H)$ curves to exemplify the criteria used to determine H_{c2} and H_{irr}.

In all superconducting materials, an H_{c2} enhancement is expected when disorder is increased (e.g., by doping). The reason is that the reduction in the electronic mean free path produces a decrease of the effective coherence length, driving the superconductor to the

"dirty limit". This effect is especially large in C-doped MgB_2, and additionally an anomalous $H_{c2}(T)$ upward curvature is also noted in the present data and reported many times. This positive curvature is related to the existence of two-gaps in MgB_2, (π-band and σ-band) and predicted by some theoretical models.

These models for a two gap superconductor in the dirty limit (Golubov et al., 2002; Gurevich, 2003) consider that nonmagnetic impurities affect the *intra*band electron diffusivities D_σ and D_π, and the *inter*band scattering rates $\Gamma_{\pi\sigma}$ and $\Gamma_{\sigma\pi}$. An implicit H_{c2} dependence on temperature can be obtained from the Usadel equations, derived taking into account only the *intra*band effect.

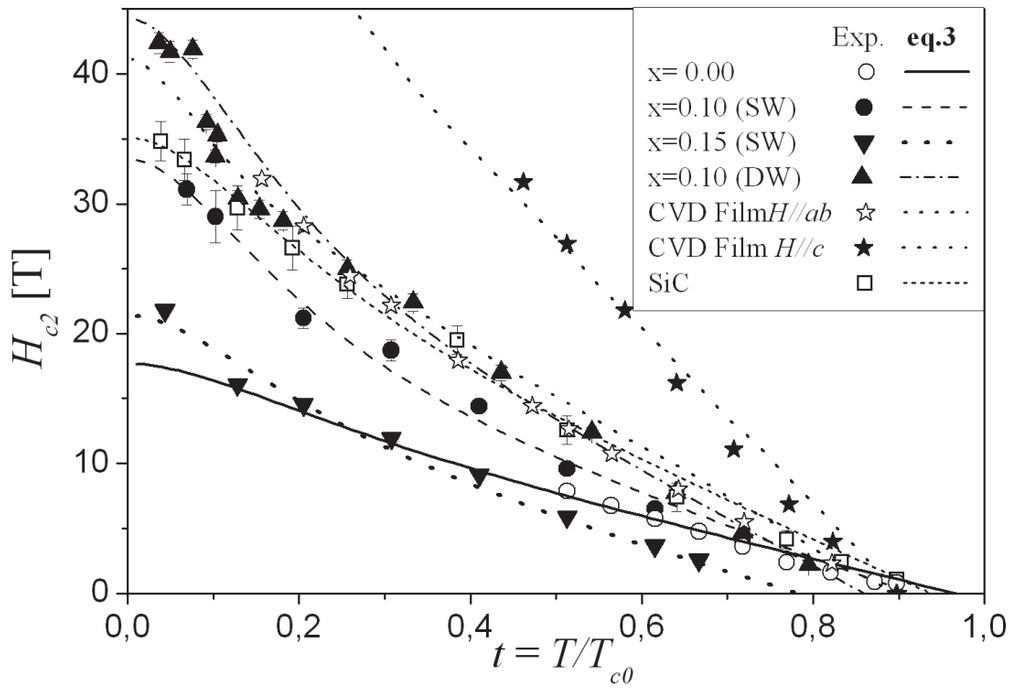

Fig. 7. Transport measurements of the upper critical field (H_{c2}) determined from the *R(H)* curves as a function of the reduced temperature $t = T/T_{c0}$, for selected samples with and without CNT addition and fit to data using equation 2 (lines). Other C-doped samples are included for comparison (Serrano et al., 2008; Braccini et al., 2005)

$$a_0\left[\ln t + U(h)\right]\left[\ln t + U(\eta h)\right] + a_2\left[\ln t + U(\eta h)\right] + a_1\left[\ln t + U(h)\right] = 0 \quad (2)$$

where, $t = T / T_{c0}$ is the reduced temperature[1],

$$\eta = D_\pi / D_\sigma ,$$

$$U(x) = \psi(1/2 + x) - \psi(1/2) ,$$

[1] In Refs. (Gurevich, 2003; Serquis et al., 2007 ; Serrano et al., 2008)) $T_{c0} = T_c(g=0)$ is defined, where g the interband scattering parameter. This value corresponds to the clean limit MgB_2 sample.

$$h = H_{c2} D_\sigma / 2\phi_0 T ,$$

$$a_0 = 0.7806$$
$$a_1 = 1.93$$
$$a_2 = 0.07$$

a_0, a_1, and a_2 were determined in ref. (Gurevich, 2003).
Another equation was derived when taking also into account the *inter*band effects:

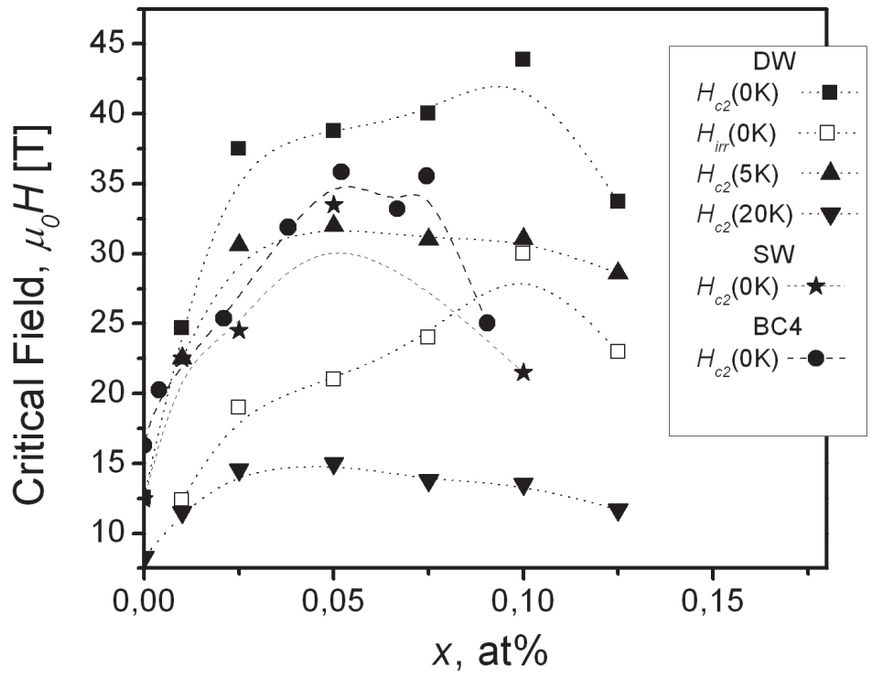

Fig. 8. The extrapolation at 0K of H_{c2} as a function of carbon content x for DW and SW CNT samples (full symbols). H_{c2} data at 5K , 20K and H_{irr}(5K) is also included for DW sample (open symbols). Lines are only guides to the eyes.

$$2w\left(\ln t + U_+\right)\left(\ln t + U_-\right) + \left(\lambda_0 + \lambda_i\right)\left(\ln t + U_+\right) + \left(\lambda_0 - \lambda_i\right)\left(\ln t + U_-\right) = 0 \tag{3}$$

where $\lambda_i = \left(\lambda_- \Gamma_- - 2\lambda_{\pi\sigma}\Gamma_{\sigma\pi} - 2\lambda_{\sigma\pi}\Gamma_{\pi\sigma}\right)/\Gamma_+$, $U_\pm = U_\pm(T, H_{c2}, D_\sigma, D_\pi, \Gamma_{\pi\sigma}, \Gamma_{\sigma\pi})$,
w, λ_0 are constants that depend on λ_{mn} (m,n = π,σ) (values obtained from *ab initio* calculations) (Golubov et al., 2002; Braccini et al., 2005).
In this case we optimized the diffusivity ratio $\eta = D_\pi / D_\sigma$ and *inter*band scattering parameter to fit the measurements using the equation (3).
Figure 7 shows the dependence of H_{c2} as a function of the reduced temperature $t = T/T_{c0}$, where T_{c0} = 39 K, of some selected samples with and without CNT addition. Other C-doped samples are included for comparison (Serrano et al., 2008; Braccini et al., 2005). The lines are fits to the data with the model proposed using the fitting parameters described above.

The upward curvature signaled as a characteristic of the presence of two gaps is apparent in these $H_{c2}(T)$ data.

Figure 8 displays the $H_{c2}(0)$ extrapolations as a function of x for DW (Serquis et al. 2007) and SW (Serrano et al. 2007) in comparison with data for other C-doped samples (Wilke et al., 2004). We observe that $H_{c2}(0)$ increases with x and has a maximum for 10 at% for DW and 5 at% for SW. For a larger x values a decrease in H_{c2} was found, probably due to a larger T_c decrease and an increase in the resistivity of the samples. Earlier MgB_2 carbon doped data (Wilke et al. 2005) also indicates an initial rapid rise for lower C contents that then slows down, reaches a maximum at intermediate carbon concentrations, and decreases for larger C contents and the same behavior was reported for MgB_2 single crystals.

The CNT additions produce a larger C incorporation than SiC, probably because of the higher synthesis temperature, resulting in samples with lower T_c. The DWCNT 10 at% sample has the highest C content into the lattice, indicating that using this kind of inclusions is an easier way to incorporate C. This allows to reach a record H_{c2} value for this sample. Earlier MgB_2 carbon doped data from Wilke *et al* (Wilke et al., 2005b) also indicates an initial rapid rise for lower C contents that then slows down, reaches a maximum at intermediate carbon concentrations, and decreases for larger C contents and the same behavior was reported for MgB_2 single crystals. The $H_{c2}(0)$ of CNTdw10 is close to the maximum H_{c2} value as a function of x. A decrease in $H_{c2}(0)$ was also observed for a larger x value (see Fig.8)), in agreement with other reported data (Senkowicz et al., 2007).

3. Effect of different kind of CNT addition on the superconducting properties of MgB_2 PIT wires and tapes

The standard and low-cost fabrication powder in-tube (PIT) method involves filling a metallic tube with superconducting powder (ex-situ) or precursors (in-situ) and drawing it into a wire and/or rolling into a tape (Flükiger et al., 2004).

MgB_2 crystallizes in the hexagonal AlB_2 type structure (space group *P6 /mmm*), and the anisotropic structure has given the motivation to investigate formation of texture by different deformation processes. A key issue on which there is no agreement in the literature is the optimization of the heat treatment parameters. Although some post-annealing appears to be necessary to achieve higher J_c, some authors reported detrimental effects of heat treatments in the performance of MgB_2 wires or tapes (Serquis et al., 2003; Goldacker, 2003; Civale et al., 2003). However, most results obtained in MgB_2 wires and tapes prepared by PIT using different kind of CNT and treated at different temperatures using several sheath materials (e.g. iron, stainless steel, Nb/Fe) indicate that the final sintering temperature is very important to improve the superconducting properties allowing carbon to be incorporated in MgB_2.

Only one work (Xu et al., 2007) studied the influence of CNT amount, reporting the effect of the "doping level" (x) in the field dependence of critical current density for MWCNT Fe-sheathed MgB_2 wires and tapes. Similarly to what was reported for bulk MgB_2 samples, they found that there is an optimum composition for all fields and temperatures studied, but the best composition for the nominal $Mg(B_{1-x}C_x)_2$ was x=0.05 and J_c decreased for x = 0.10 (see Figure 9). However, many other researchers focused in which was considered the best composition x=0.10 studying the influence of other parameters:

- the effect of CNT type (Kováč et al., 2007) in comparison with other C-compounds (SiC, graphite)

- the effect of MWCNT size and sintering temperature (Kim et al., 2006a, 2006b, 2006c)
- the effect of sintering temperature when using SW CNT (Kim et al., 2007)
- the possibility of MW CNT alignment by mechanical drawing in the PIT process (Dou et al., 2006).

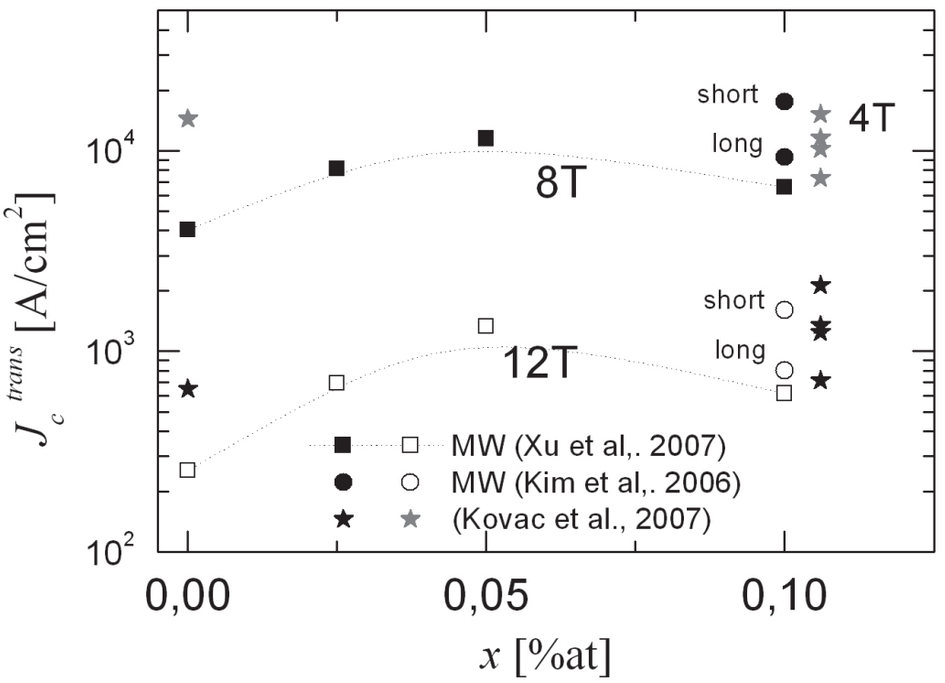

Fig. 9. Critical current density as a function of MW CNT content measured by transport in Fe-sheath $Mg(B_{1-x}C_x)_2$ wires at 8 T (black symbols) and 12 T (open symbols) (Xu et al., 2007). For comparison were included data from Fe/Nb sheath tapes with 5%wt addition of different CNT types (Kováč et al., 2007) and short and long MW CNT MgB_2 wires (Kim et al., 2006b)

To illustrate the effect of some of the mentioned parameters we plotted in Figure 10 the critical current density of

- Left side: MgB_2 /Fe-Nb tapes with 5%wt addition of different CNT types (Kováč et al., 2007). SW: Arc discharge single wall nanotubes; SW-D: Purified arc discharge single wall nanotubes, Dry-mixed; SW-W: Purified arc discharge single wall nanotubes, Wet-mixed; MW: Multi wall carbon nanotubes (~60 nm × 1 μm). For comparison were included the pure (0) and a MgB_2 tapes with 5%wt addition of SiC. This last addition is more effective in the whole field range in agreement with bulk results, while all CNT types only enhance J_c for high fields. The normalized current densities (shown in Figure 11) allow better comparison between the slopes of $J_c(\mu_0 H)$, indicating a positive effect for all additions. This field dependence enhancement is ascribed to the effect of C-incorporation, which increases the upper critical field. The decrease of T_c corresponding to a higher C-doping effect can be observed in the inset of Figure 9.
- Right side: MgB_2/Fe wires with aligned MW CNT measured along (a) and perpendicular (c) to the wire (Dou et al., 2006). While the pure sample has little differences between both measurement field directions, there is a clear difference in

samples with MW addition, which increased with field. This is a good indication that CNTs could be aligned along the longitudinal axis of the MgB_2 wires by mechanical drawing in the PIT process.

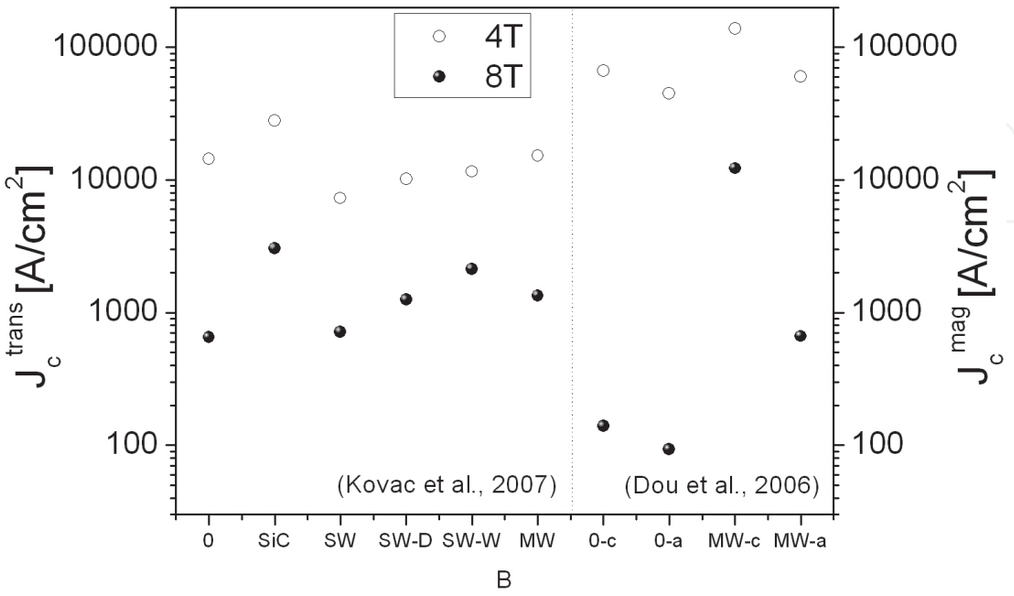

Fig. 10. (Left) Critical current density measured by transport in MgB_2 /Fe-Nb sheath tapes with 5%wt addition of different CNT types (Kováč et al., 2007) at 8 T (black symbols) and 4 T (open symbols). (Right) Critical current density measured by magnetization in Fe sheath MgB_2 wires with aligned MW CNT measured along (a) and perpendicular (c) to the wire (Dou et al., 2006)

Matsumoto (Matsumoto et al., 2006) reported that J_c in SiC-alloyed MgB_2 tapes depends on a complex relation between grain connectivity, H_{c2}, and flux pinning induced by grain boundaries and precipitates. However, the distinct effect of C incorporation through different routes in J_c and H_{c2} is still not entirely understood.
Matsumoto *et al* reported a similar $H_{c2}(0)$ to our record value for a SiC-doped MgB_2 tape prepared by the PIT method. These results correspond to a PIT tape sample that probably has some texturing and the reported H_{c2} data was measured with the applied field parallel to the tape. Since we measured randomly oriented polycrystalline bulk samples, our results cannot be easily compared with Matsumoto's.

4. Effect of CNT addition on the magnetic relaxation of MgB_2

4.1 Introduction

In Section 2.2 we have shown that the main effect of DW CNTs addition is the simultaneous increase in the critical current density and the upper critical field H_{c2}. However, it is not clear if these two effects are connected. In fact, the vortex physics underlying this performance improvement has not been so far understood. In this section, we present a very recent work (Pasquini et al., 2011), where the role of CNT addition is investigated by studying the magnetic relaxation in bulk MgB_2 samples.

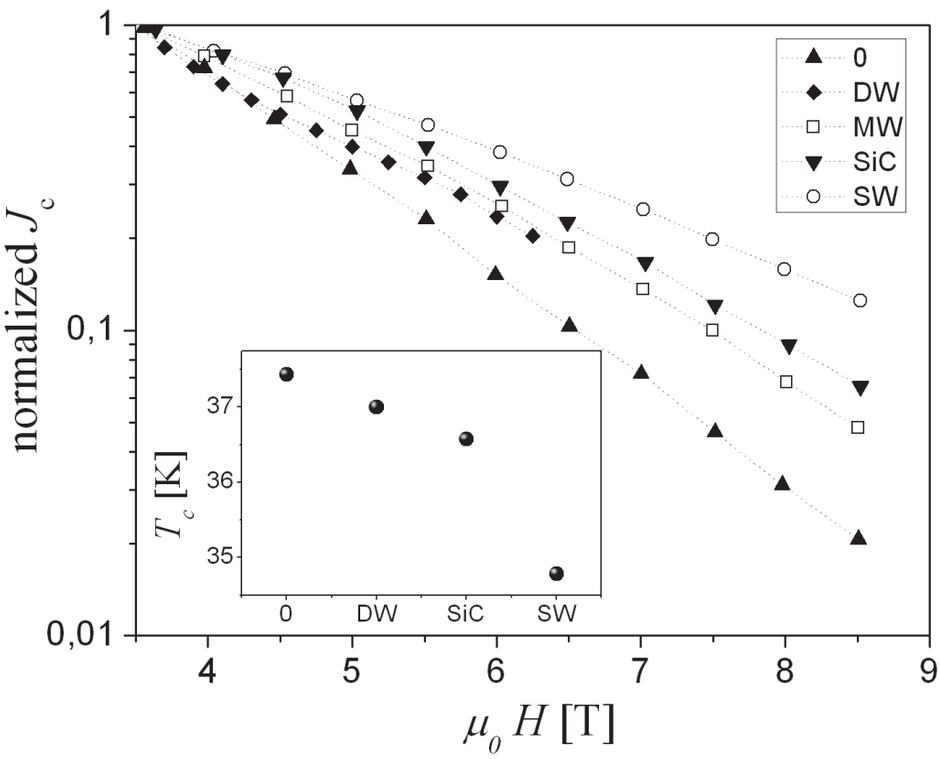

Fig. 11. Normalized critical current densities $J_c(\mu_0 H)/J_c(3.5\ T)$ showing the difference in slope for a pure sample and MgB_2 tapes with 5%wt addition of different CNT types (Kováč et al., 2007), including a DW with similar content (Serquis et al., 2011). The inset shows the T_c of the same tapes.

As was mentioned in Section 2.1.1, if a superconducting sample is fully penetrated by the magnetic field B, the magnetization m is proportional to the density current J flowing in the sample that, in the ideal critical state approximation is the critical current density J_c. However, due to the thermal activated motion, this "measurable" critical current is lower than the "true" J_{c0}. The main quantity governing the creep of vortices is the activation barrier U(J,T,B). In a magnetic relaxation experiment both the magnetization m and J_c decay in time as

$$-\frac{\partial J_c}{\partial t} = C_j\, e^{\frac{-U(J_c,T,B)}{kT}}$$

and then

$$-\frac{\partial m}{\partial t} = C_m\, e^{\frac{-U(j_{(m)},T,B)}{kT}} \tag{4}$$

where $C_c \sim J_c/\tau_0$ or $C_m \sim m/\tau_0$ can be approximated as constants.
The activation barrier is expected to be described by the general expression (Blatter et al.,1994; Geshkenbein et al., 1989)

$$U(J;T;B)=\frac{U_c(T,B)}{\mu}[(\frac{J_{c0}(T,B)}{J})^{\mu}-1] \quad (5)$$

where $U_c(T,B)$ is the pinning energy and μ is a critical exponent characteristic of the particular creep regime.

In High Temperature Superconductors (HTSs), the creep drastically reduces the measured current density, so $J_c<<J_{c0}$. A large number of glassy creep regimes in this limit have been proposed theoretically (Blatter et al., 1994; Yeshurum et al., 1996) and many of them observed experimentally (Thompsom et al., 1994, 1997), where $U(J,T,B)\cong g(T,B)J^{-\mu}$.

In those cases the temperature dependence of the measurable J_c is dominated by creep while the $J_{c0}(T)$ dependence is negligible. On the other hand, in traditional type II superconductors the current decay is very small, so $(J_{c0}-J_c)<<J_{c0}$, therefore equation (5) take the traditional Anderson-Kim (A-K) linear dependence (Anderson et al., 1964)

$$U(J,T,B)\cong U_c(T,B)(1-\frac{J}{J_{c0}(T,B)}) \quad (6)$$

In these very low creep superconductors an experimental confirmation of glassiness, which regardless of the specific approach always involves detecting tiny deviations from the Anderson-Kim model, is extremely challenging.

From this basic point of view, MgB_2 is a very particular system, as the intermediate T_c and moderate anisotropy makes the creep effects smaller than in HTS but larger than in conventional superconductors. The influence of thermal fluctuations in the vortex physics is measured by the Ginzburg number $G_i=(1/2)(kT_c/H_c^2\xi^3\gamma^{-1})^2$. For $YBa_2Cu_3O_{7-\delta}$ this is as large as $G_i \sim 10^{-2}$, and even larger for the more anisotropic Bi-based compounds, while for NbTi, the paradigmatic strong-pinning conventional superconductor, $G_i \sim 10^{-8}$. For MgB_2, depending on the doping level we have $G_i \sim 10^{-4}$-10^{-5}. This is just in the middle between the extreme cases. The first consequence is that in magnetization measurements, the A-K limit is not necessary valid in the whole temperature range, and the measured J_c is expected to be in the intermediate range $(J_{c0}-J_c)\lesssim J_c$.

In the rest of the section we present a creep study in bulk MgB_2 samples as-grown and doped with different doses of carbon nanotubes. In subsection 4.2 experimental relaxation rates are presented, and the general behaviour is described. In subsection 4.3 we review some fundamental concepts and formulas concerning creep rates and activation energies to perform in subsection 4.4 a careful analysis of results that allows us to identify the region where the A-K model is valid. In 4.5, the pinning energies U_c, true critical current densities J_{c0}, and correlation volumes V_c are estimated and compared. Conclusions are summarized in 4.6.

4.2 Relaxation rates

Samples used in this study were prepared by solid-state reaction with magnesium (-325 mesh, 99%) and amorphous boron (99%) as starting materials (Serrano et al., 2008). The powders were ground inside a glove box and pressed under 500 MPa into small pellets with dimensions of 6 mm in diameter and 4 mm in thickness, wrapped together with extra 20%at Mg turnings (99:98% Puratronic) in Ta foil and then placed in an alumina crucible inside a tube furnace in flowing Ar=H_2 at 900C for 30 min.

The relaxation measurements were carried out in a Quantum Design model MPMS XL 7T SQUID based magnetometer. Time-dependent data were taken with a protocol similar to that described in ref. (Civale et al., 1996). A scan length of 3 cm was used in order to minimize the effects due to the non-uniformity of the applied magnetic field that was applied parallel to the longest axis of the sample. For each relaxation measurement, the samples were first cooled and stabilized at the measurement temperature. Then the field was first raised up to 6T and then lowered to the measuring field to assure that the sample was fully penetrated. Intermediate measurements were performed in the upper and lower magnetization branches to subtract the reversible magnetization. We checked for and ruled out any effects due to the magnet self relaxations (H variations during the measurement time) that could lead to spurious changes in the magnetization of the samples.

The experimental critical current density $J_c(t)$ has been calculated from the measured magnetic moment using equation (1), as in previous sections.

As reported in section 2.2., the response for samples with DWCNT additions between 1% and 10% at temperature far below T_c is very similar and the "measured" critical current density J_c is optimal in this range of doping. This fact is illustrated in Figure 3, where J_c obtained from typical magnetization loops in samples with different doses of DWCNT is plotted as a function of the applied magnetic field H at T = 5K and 20K . The response for samples with 1 at% and 10 at% addition of DWCNT is very similar. At low temperature (5 K), CNT addition enhances J_c more than twice for all the measured range of H. On the other hand, at high temperature (20 K) the response of pure and CNT samples is quite similar but CNT addition continues being efficient at fields higher than H = 2T.

The magnetic relaxation has been measured in pure MgB_2 samples and samples with DWCNT doses between 1 at% and 10 at% in the range between 5K and 25K. The corresponding relaxation rate $S=-d(\ln(J))/d(\ln(t))$ has been obtained as the slope of the $\ln J$ vs $\ln t$ graph. Results for H =1T (full symbols) and 3T (open symbols) are shown in Figure 12.

Samples with doses of 2.5% and 5% of carbon nanotubes have also been measured and display similar results, not shown in the figure for clarity.

As was described in the introduction, the S values are intermediate between those measured in low and high T_c materials. With this moderate relaxation, the temperature dependence of $J_c(t)$ (Figure 3) cannot be explained assuming a T independent J_{c0} at low temperature. An intrinsic $J_{c0}(T)$ dependence must to be taken into account.

Again, at H = 1 T the decay in time is quite similar in all the doped samples with doses between 1% and 10%. However, same unexpected results appear. The $S(T)$ curve at H=3T is similar for pure and CNT samples in all the temperature range. Furthermore, at H=1T the pure sample that has a lower J_c (associated with a lower pinning) has also a lower relaxation (associated with a higher pinning energy U_c).

We have proceeded to analyze the relaxation data in a pure and a 10 at% CNT samples to get an understanding of the causes of this puzzle. The procedure and results are described in the subsections 4.3 and 4.4.

4.3 Creep and activation energies in the Anderson-Kim approximation

In the general case (Blatter et al., 1994), the relaxation rate S is related with the pinning energy by

$$\frac{1}{S} = \frac{U_c(T,B)}{kT} + \mu \ln(1 + t/t_0) \sim \frac{U_c(T,B)}{kT} + \mu \ln(t/t_0) \qquad (7)$$

if $t >> t_0$. This expression should be valid in all the current range, including the A-K limit. Therefore, if U_c is T independent at low temperatures, a linear relationship between *1/S* and *1/T* is expected.

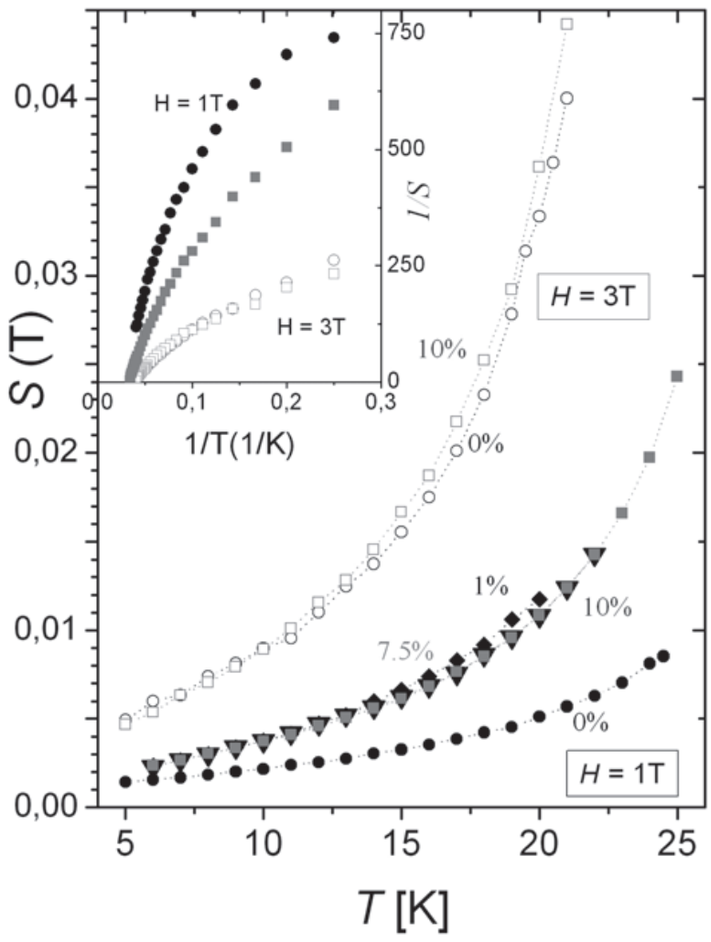

Fig. 12. Relaxation rate S as a function of temperature for a pure MgB_2 sample (circles) and for samples with different doses of DWCNT: 1% (diamonds), 7.5% (triangles) and 10%(squares) at H = 1 T (full symbols) and H = 3T (open symbols). In the inset, the plot of *1/S* vs. *1/T* reveals that it is not possible to assume a temperature independent pinning energy at low temperature in all the cases.

As was mentioned in the introduction, the A-K approximation assumes $(J_{c0} - J) << J_{c0}$ or $(J / J_{c0}) \sim 1$, that lets to the linear dependence of eq. (6) between the activation barrier U and the density current J. The integration of eq. (4) in this limit gives the well known logarithmic decay of the experimental critical current density with time.

$$\frac{J_c(t)}{J_{co}(T,B)} \sim [1 - \frac{kT}{U_c(B,T)} \ln(t/t_o)] \tag{8}$$

and allows to estimate $U_c(T,B) / kT$ under the supposition that $J \sim J_{c0}$.

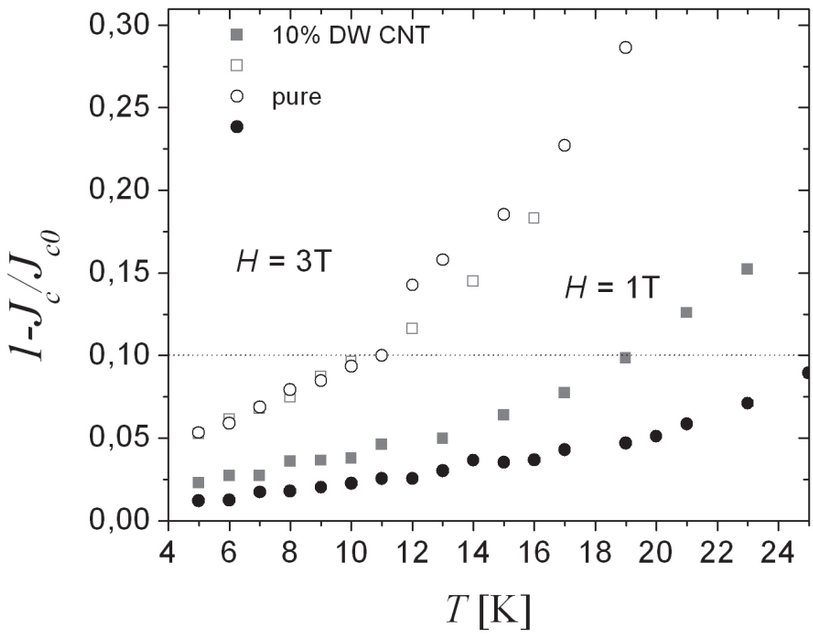

Fig. 13. Ratio $\Delta J/J_{c0}$ as a function of temperature for pure (circles) and 10% CNT (squares) samples at H = 1T (full symbols) and H=3T (open symbols). $\Delta J = J_{c0} - J_c$ is the difference between the estimated "true" critical current density (see text) and the measured critical current density. A criterion of 10% (doted line) has been taken to validate the A-K approximation $\Delta J << J_{c0}$.

An alternative method combines eqs. (4) and (6) to obtain a linear dependence between J and $\partial J/\partial t$ that, under the condition $\ln C_J << U_c(T,B)/kT$ results in (Pasquini et al., 2011)

$$J_c(t) = \frac{kT\,J_{co}(T,B)}{U_c(t,B)} \ln\left|\frac{dJ}{dt}\right| + J_{co}(T,B) \tag{9}$$

Due to the numerical differentiation, this method has a greater error in the calculation of the pinning energy, but allows estimating $J_{c0}(B,T)$.

A mayor difficulty to directly decide the validity of the A-K approximation from the relaxation data at a single temperature is the extremely large time needed to reliably determine the linear relationship (8) (i.e. the logarithmic decay with time of the current density). However, the resulting fitting parameter $J_{c0}(B,T)$ must be consistent with the A-K assumption $(J_c / J_{c0}) \sim 1$ and the resulting fitting parameter $U_c(T,B)$ must be consistent with eq. (7). If these two conditions are not fulfilled then some of the assumptions was wrong and we can conclude that the AK description is not valid.

In the following section, we apply the above procedure to MgB_2 relaxation data, determining the temperature region where results are consistent.

4.4 Data analysis in MgB_2 samples

As can be observed in the inset of Figure 12, it is not possible to identify in all the cases a low T region with a linear relationship between 1/S and 1/T, characteristic of a temperature independent pinning energy. For this reason, experimental data where separately analysed

at each temperature **assuming** a linear dependence between U and J, i.e. the validity of the A-K approximation.
At each temperature $J_c(t)$ has been plotted has a function of $ln\ t$ and $ln\ (-\partial J/\partial t)$. The fitting parameter $A(T) = (kTJ_{c0}(T))/U_c(T))$ has been extracted from the slope using equations (8) and (9), and $J_{c0}(T)$ from the intercept using eq. (9) (Pasquini et al., 2011).
In Figure 13 the estimated true critical current density J_{c0} is compared with the measured critical current density J_c (the first point measured in the $J_c(t)$ relaxation) by plotting $(J_{c0}-J)<<J_{c0}$ as a function of temperature for a pure and a 10%doped sample, at H=1 T and 3T.
Taking a 10% criterion to determine the limit of the A-K condition $(J_{c0}-J)<<J_{c0}$, the resulting $J_{c0}(t)$ is consistent below the temperature where each experimental curve crosses the doted horizontal line.
In figure 14 the resulting pinning energies obtained from the slope of eq. (8) (squares) and eq. (9)(circles) are plotted as a function of temperature and compared with T/S (asterisks) for a pure and a 10%doped sample, at H=1 T and 3T. Results have been restricted to the consistent T region obtained by the above analysis.

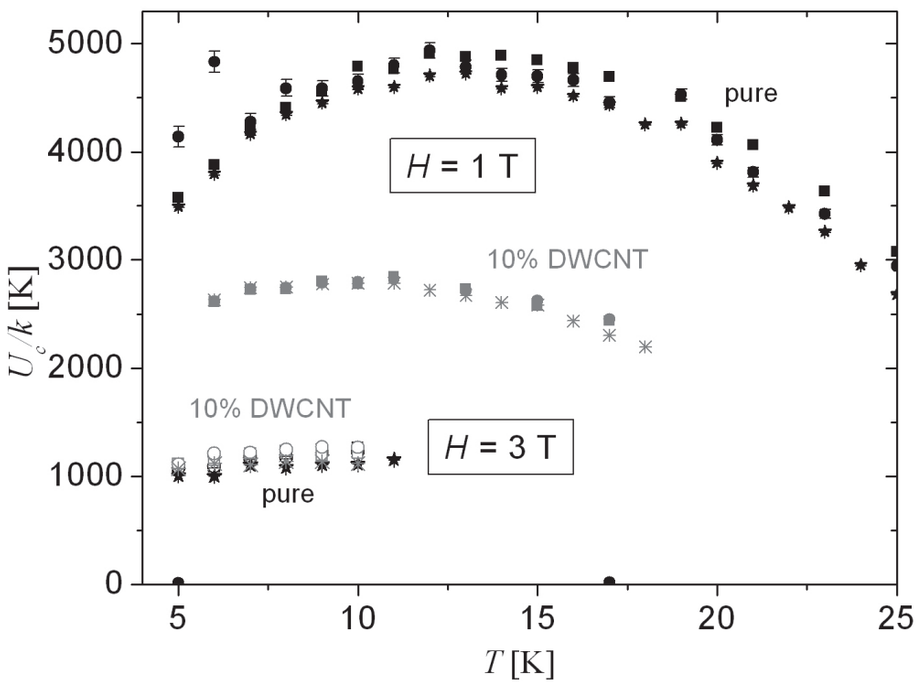

Fig. 14. Estimated pinning energies U_c/k as a function of temperature for pure (black symbols) and 10% doped (gray symbols) samples at H = 1T (full symbols) and H = 3T (open symbols) from the slope of eq. (8) (circles) and eq. (9) (squares). Asterisks indicate the calculated T/S in each case. Results shown are limited to the region where the A-K approximation is consistent.

As can be observed (with exception of the lower temperatures data in the undoped sample at H= 1 T) pinning energies obtained from the three methods are very similar, and this validates the fitting procedure, including the estimation of $J_{c0}(T)$ from eq. (9).
Observing the resulting T dependence in Figure 14 it seems that, in most of the cases, pinning energies remain nearly constant at low temperatures. The unexpected drop in U_c at

the lower temperatures data in the undoped sample at H= 1 T, together with the inconsistence of the analyzed data, could imply the presence of another relaxation mechanism, perhaps associated with macroscopic flux jumps. In the data measured at H=1 T a drop at a higher temperature far below the irreversibility line is also observed.
On the other hand, a continuous decrease occurs in the critical current density. This can be observed in figure 15, where the true critical current density is plotted in the studied range for the same samples.
The previous analysis excludes the creep study in the high temperature region using the A-K approximation. Successful procedures have been developed to analyze creep data in high T_c superconductors (Maley et al., 1990; Civale et al., 1996) in the limit $J_c << J_{c0}$, but they are not suitable for intermediate creep regime. However, in the present subsection we showed that, from the present study at low temperatures, a good insight about the role of doping can be obtained.

4.5 Discussion

Consistent with the relaxation rates, at H=1 T there is a clear decrease of U_c after CNT addition, whereas at H=3 T the doping has not an evident effect in the pinning energies.
The parameter U_c is associated with the pinning energy of a pinning volume that, in a single vortex pinning regime, is defined by the disorder parameter $\gamma(T)$ and the superconducting coherence length $\xi(T)$ (Blatter et al., 1994). In section 2.2 we have shown that DWCNT addition enhances $H_{c2}(T)$ by doping the B site, i.e. reduces $\xi(T)$. On the other hand, it is expected that doping increases disorder. Therefore, these two consequences of DWCNT doping will compete and define the effect in the pinning energies and critical currents.

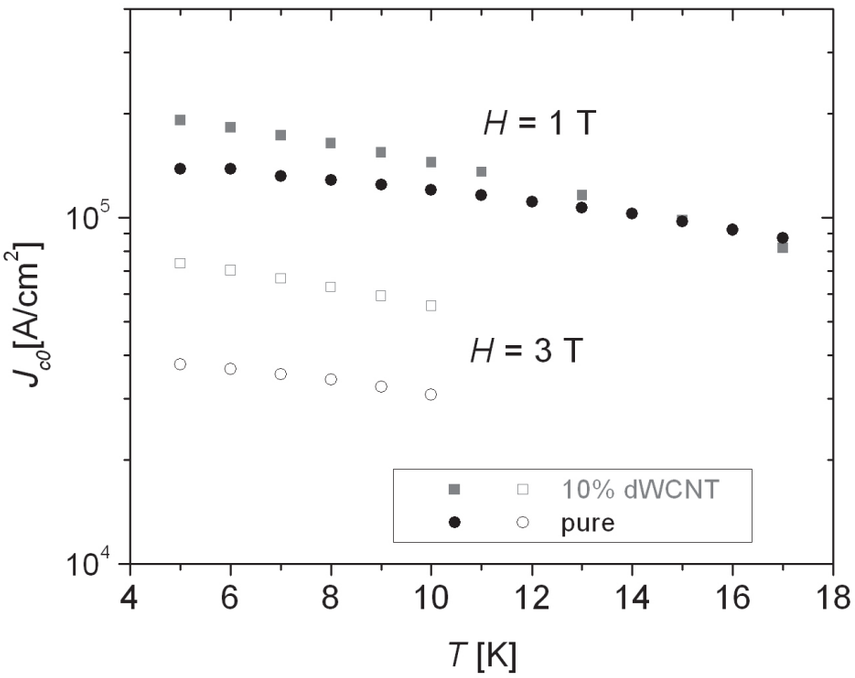

Fig. 15. Estimated critical current density J_{c0} as a function of temperature for pure (circles) and 10% CNT (squares) samples at H = 1T (full symbols) and H=3T (open symbols).

The fact that the doping effect in the pinning energies is field dependent is a clear indication of a collective pinning regime.

In a collective regime, the pinning volume is determined by the competition between elastic and pinning energies and each volume V_c of the vortex system is collectively pinned with energy U_c. The Lorentz force over a volume V_c is $F_L \sim (1/c)BJ\ V_c$ and, in a rough estimation, the pinning force is $F_p \sim U_c/\xi$. When J reaches the critical current density J_{c0}, the pinning and Lorentz forces are balanced and therefore the following relationship is obtained:

$$V_c(T,B) \sim \frac{c\,U_c(B,T)}{B\,\xi(T)J_{co}(B,T)} \tag{10}$$

In section 2.2, we have presented H_{c2} measurements in pure and DWCNT MgB_2 samples and we have found (Serquis et al., 2007) that $H_{c2}(T)$ fits very well the function proposed in ref (Braccini et al,. 2005). We have estimated ξ(T) from $H_{c2}(T)$ for the as grown samples and for samples with 10% DWCNT. Using this $\xi(T)$ dependence we have estimated $V_c(T,B)$ from our data. Results are shown in Figure 16, where V_c is plotted as a function of temperature a $H(T)$ = 1 T (right axis) and 3 T (left axis) for both samples.

The estimated numerical values (~10^{-15} cm^3) imply that the correlation radius is larger than the main vortex distance, in agreement with a collective pinning regime of vortex bundles.

Doping additionally reduces the correlation volume, consistent with the increase in the critical current density.

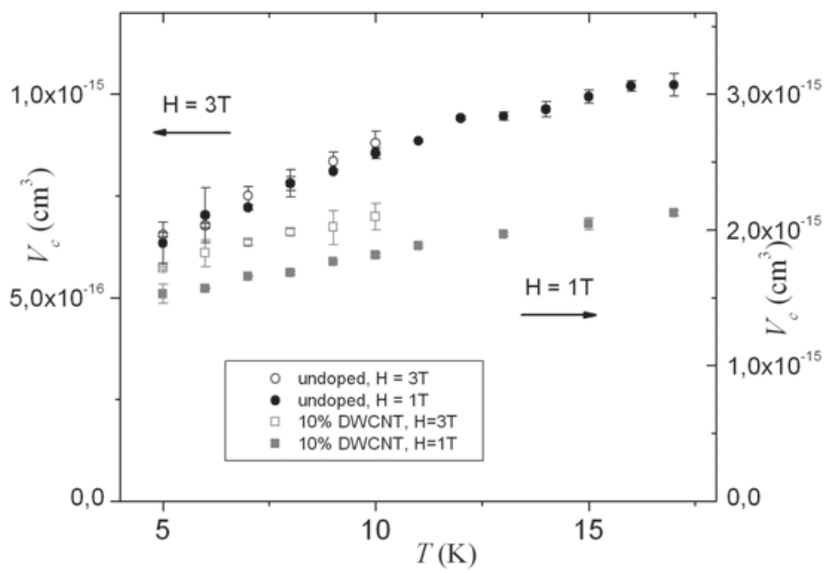

Fig. 16. Estimated collective pinning volume V_c as a function of temperature for pure (circles) and 10% DWCNT (squares) samples at H = 1T (full symbols, left axis) and H=3T (open symbols, right axis).

From the comparison of data taken at H = 1 T and 3 T, in both pure and CNT samples, the correlation volume at H= 3T is approximately three times smaller than that obtain at H = 1 T

and both J_{c0} and U_c decrease with B. This field dependence for U_c does not correspond with that predicted by the classical collective pinning theory for the activation energy of vortex bundles when pinning arises from random point defects (Blatter et al., 1994). However, this discrepancy is not surprising, as we know that the strong pinning in these MgB_2 samples arises from a variety of larger defects rather than atomic-size disorder.

4.6 Conclusions

Magnetic relaxation in bulk MgB_2 samples as-grown and with DWCNT doses between 1% and 10% in the range between 5K and 25K has been measured and the corresponding critical current density has been calculated. The current decay in time is quite similar in all the doped samples with doses between 1% and 10%.

A careful creep analysis has been carried out in a pure sample and in one with 10% of carbon nanotubes at H= 1 T and 3 T.

The analysis has been performed under the Anderson-Kim approximation, valid in the limit where the measured critical current density J_c is similar to the "true" one J_{c0} that would be present in the absence of creep phenomena. In these samples, even at the loweest temperatures it is necessary to include an explicit field and temperature dependence of both the pinning energies $U_c(T,B)$ and true critical current densities $J_{c0}(T,B)$.

These pinning properties have been obtained as fitting parameters from the experimental data for two different methods. The consistence of the fitting parameters with the A-K limit has been required to delimit the region of validity of the analysis.

In the valid region, the pinning energies and critical current densities have been estimated and compared. The dependence with magnetic field, together with numerical estimations of the pinning volume, indicate the presence of a collective pinning regime of vortex bundles. There is a decrease in the pinning energies that implies an increase in the relaxation rates as a consequence of DWCNT addition. However, the true critical current densities increase, due to a decrease in the collective pinning volumes.

We conclude that the origin of the main changes in the pinning properties with doping are the reduction of the coherence length (that decreases the pinning energies) and the increase in the disorder parameters (that increase the critical current and decrease the pinning volume).

The strong temperature dependence of the coherence length is probably the main reason to the observed temperature dependence in the pinning properties. At the lower temperatures, thermal instabilities that originate macroscopic flux jumps could also play a role.

A method to analyse the relaxation data in the high temperature region, beyond the A-K approximation, is necessary and will be object of a future work.

5. Summary

The effect of carbon substitution is one of the most studied in MgB_2 and the results on C solubility and the effects of C-doping on T_c, J_c and H_{c2} reported so far vary significantly due to precursor materials, fabrication techniques and processing conditions used. The distinct effect of C incorporation through different routes using various CNT types leads to a simultaneous improvement in J_c and H_{c2}, but their effectiveness change with temperature or applied field according to each type of addition. This effect was reported in many works, not only for bulk samples but also for wires and tapes prepared by PIT method.

The reason for this is the dual role of the CNT. They partially dilute into the MgB_2 matrix, acting as a source of C that increases H_{c2}. In fact, the highest H_{c2} values observed so far in bulk MgB_2 correspond to a 10% addition of DWCNT, which present a high level of C doping. At the same time, the fraction of the CNT that retain their structural integrity are ideally suited to act as strong vortex pinning centers due to their tubular geometry and their diameter close to the superconducting coherence length of MgB_2, producing a large J_c enhancement. As an additional result, the measured H_{c2} vs T in all samples are successfully described using a theoretical model for a two-gap superconductor in the dirty limit (Gurevich, 2003). This has strong fundamental impact, as it provides clear evidence in support of the basic scenario currently used to describe the superconducting behavior of MgB_2, and opens a path for future research in H_{c2} enhancement.

The study of the magnetic relaxation of MgB_2 with and without DWCNT bulk samples can give some insight about the possible correlation in the simultaneous increase in the critical current density and the upper critical field. The experimental relaxation rates showed that the pure sample that has a lower J_c (associated with a lower pinning) has also a lower relaxation (associated with a higher pinning energy U_c). To understand these results the relaxation data was described and analyzed under the Anderson-Kim frame model (Anderson, 1964). The pinning energies U_c, true critical current densities J_{c0}, and correlation volumes V_c were estimated and compared. The strong temperature dependence of the coherence length is probably the main reason to the observed temperature dependence in the pinning properties with CNT additions: the reduction of the coherence length (that decreases the pinning energies) and the increase in the disorder parameters (that increase the critical current and decrease the pinning volume).

6. Acknowledgment

Research supported by CONICET, UNCuyo, UBACyT, and MinCyT-PICT (AS, GP) and by the U.S. Department of Energy, Basic Energy Sciences, Materials Sciences and Engineering Division (LC).

7. References

Anderson, P.W. & Kim, Y.B. (1964). Rev. Mod. Phys. 36, 39

Avdeev, M.; Jorgensen, J. D.; Ribeiro, R. A.; Bud'ko, S. L. & Canfield, P. C. (2003). Physica C 387, 301-306

Ban, E.; Sakaguchi, R.; Matsuoka, Y.; Goto, T.; Watanabe, K. & Nishijima, G. (2005). Physica C, vol. 426–431, pp. 1249–1253

Bean, C. P. (1962). Phys. Rev. Lett 8, 250-253

Blatter, G.; Feigel'man, M. V.; Geshkenbein, V. B.; Larkin, A. I. & Vinokur, V. M. (1994). Rev. Mod. Phys. 66, 1125

Braccini, V.; Gurevich, A.; Giencke, J. E.; Jewell, M. C.; Eom, C. B.; Larbalestier, D. C.; Pogrebnyakov, A.; Cui, Y.; Liu, B. T.; Hu, Y. F.; Redwing, J. M.; Li, Qi; Xi, X. X.; Singh, R. K.; Gandikota, R.; Kim, J.; Wilkens, B.; Newman, N.; Rowell, J.; Moeckly, B.; Ferrando, V.; Tarantini, C.; Marré, D.; Putti, M.; Ferdeghini, C.; Vaglio, R. & Haanappel, E. (2005). Phys. Rev. B 71, pp. 012504-012508

Brinkman A.; Golubov A. A.; Rogalla H.; Dolgov O V.; Kortus J.; Kong Y.; Jepsen O & Andersen O K (2002). Phys. Rev. B 65, 1805171-1805174

Buzea C. & Yamashita T. (2001). Supercond. Sci. Technol. 14, R115-R146

Cheng C. H.; Zhang H.; Zhao Y.; Feng Y.; Rui X. F.; Munroe P.; Zeng H. M.; Koshizuka N. & Murakami M. (2003). Supercond. Sci. Technol. 16, 1–5

Civale L.; Pasquini G.; Levy P.; Nieva G.; Casa D & Lanza H. (1996). Physica C 263, 389

Civale L.; Serquis A.; Hammon D. L.; Liao X. Z.; Coulter J. Y.; Zhu Y. T.; Holesinger T.; Peterson D. E. & Mueller F. M. (2003). IEEE Trans Appl. Supercond .13, 3347-3350.

Dou S. X.; Yeoh W K.; Horvat J & Ionescu M (2003). Appl Phys Lett 83, 4996-4998

Dou S. X.; Yeoh W. K.; Shcherbakova, O.; Wexler, D.; Li Y.; Ren, Z. M.; Munroe P.; Chen, S. K.; Tan, K. S.; Glowack B. A. & MacManus-Driscoll, J. L. (2006). Advanced Materials, 18, 785-788

Flükiger R.; Suo HL.; Musolino N.; Beneduce C.; Toulemonde P & Lezza P (2003). Physica C 385, 286-305, & references therein

Geshkenbein V. B.; Feigelman M.V & Vinokur V. M (1989). Physica C 162-164, 239

Goldacker et al (2004). Supercond. Sci. Technol. 17, S490-S495

Goldacker W et al, in: A. Narlikar (Ed.) (2002). Studies of High Temperature Superconductors Vol. 45, Nova Science Publishers, New York

Golubov A. A.; Kortus J.; Dolgov O. V.; Jepsen O.; Kong Y.; Andersen O. K.; Gibson B. J.; Ahn K. & Kremer R. K. (2002). J. Phys: Condensed Matter 14, 1353-1360

Gurevich A. (2003). Phys. Rev. B 67, 184515-184528

Gurevich A.; Patnaik S.; Braccini V.; Kim K. H.; Mielke C.; Song X.; Cooley L. D.; Bu S. D.; Kim D. M.; Choi J. H.; Belenky L. J.; Giencke J.; Lee M. K.; Tian W.; Pan X. Q.; Siri A.; Hellstrom E. E.; Eom C. B. & Larbalestier D. C. (2004). Supercond. Sci. Technol. 17, 278–286

Häβler W.; Herrmann M.; Rodig C.; Schubert M.; Nenkov K. & Holzapfel B. (2008) Supercond. Sci. Technol. 21, 062001

Kazakov S M.; Puzniak R.; Rogacki K.; Mironov A. V.; Zhigadlo N D.; Jun J.; Soltmann Ch; Batlogg B & Karpinski J (2005). Phys. Rev. B 71, 024533-024543

Kim, J.H.; Yeoh, W.K.; Qin,M.J.; Xu, X.; Dou, S.X.(2006a). J. Appl. Phys. 100, 01390

Kim, J.H.; Yeoh, W.K.; Qin,M.J.; Xu, X.; Dou, S.X.; Munroe,P.; Kumakura,H.; Nakane,T.; Jiang, C.H.(2006b) Applied Physics Letters 89, 122510

Kim, J.H.; Yeoh, W.K.; Qin,M.J.; Xu, X.; Dou, S.X.; Munroe,P.; Rindfleisch, M.; Tomsic, M. (2006c). Physica C, 449, 133–138

Kim, J.H.; Yeoh, W.K.; Xu, X.; Shi M.J. & Dou, S.X. (2007). IEEE Transactions on Applied Superconductivity 17, 2907-2910

Kováč P. ; Hušek I.; Skákalova V.; Meyer J.; Dobročka, E.; Hirscher, M. & Roth, S. (2007). Supercond. Sci. Technol. 20, 105–111

Larbalestier D. C.; Cooley L. D.; Rikel M. O.; Polyanskii A. A.; Jiang J.; Patnaik S.; Cai X. Y.; Feldmann D. M.; Gurevich A.; Squitieri A. A.; Naus M. T.; Eom C. B.; Hellstrom E. E.; Cava R. J.; Regan K. A.; Rogado N.; Hayward M. A.; He T.; Slusky J. S.; Khalifah P.; Inumaru K. & Haas M. (2001). Nature (London) 410, 186-189

Lee S.; Masui T.; Yamamoto A.; Uchiyama H & Tajima S (2003). Physica C 397, 7-13

Ma Y.; Zhang X.; Nishijima G.; Watanabe K.; Awaji S. & Bai, X. (2006). Appl. Phys. Lett, vol. 88, pp. 072502–072504

Maley M. P.; Willis J. O.; Lessure H. & McHenry M. E. (1990). Phys. Rev. B. 42, 2639
Matsumoto A.; Kumakura H.; Kitaguchi H.; Senkowicz B J.; Jewell M C.; Hellstrom E E.; Zhu Y.; Voyles P. M. & Larbalestier D. C. (2006). Appl. Phys. Lett. 89, 2508-2510
Nagamatsu J.; Nakagawa N.; Muranaka T.; Zenitani Y. & Akimitsu J. (2001). Nature (London) 410, 63-64
Pasquini G.; Serquis A.; Moreno A.; Serrano G.; Civale L. (2011). Preprint
Putti M.; Braccini V.; Ferdeghini C.; Pallecchi I.; Siri A. S.; Gatti F.; Manfrinetti P. & Palenzona A. (2004). Phys. Rev. B 70, 052509-052513
Senkowicz B J.; Giencke J E.; Patnaik S.; Eom C B.; Hellstrom E. E. & Larbalestier D. C. (2005). Appl. Phys. Lett .86, 202502-202505
Senkowicz B J.; Polyanskii A.; Mungall R J.; Zhu Y.; Giencke J. E.; Voyles P M.; Eom C B.; Hellstrom E. E. & Larbalestier D. C. (2007). Supercond. Sci. Technol .20, 650
Serquis A.; Civale L.; Hammon D. L.; Coulter J. Y.; Liao X. Z.; Zhu Y. T.; Peterson D. E. & Mueller F M (2003). Appl. Phys. Lett 82, 1754
Serquis A.; Serrano G.; Moreno M S.; Civale L.; Maiorov B.; Balakirev F. & Jaime M (2007). Supercond Sci. Technol. 20, L12–L15
Serrano G.; Serquis A.; Dou S. X.; Soltanian S.; Civale L.; Maiorov B.; Balakirev F. & Jaime M. (2008). Journal of Applied Physics 103, 023907
Serrano G.; Serquis A.; Civale L.; Maiorov B.; Holesinger T.; Balakirev F. & Jaime M. (2009). International Journal of Modern Physics B 23, 3465-3469
Shekhar C.; Giri R.; Malik S. K. & Srivastava O. N. (2007). Journal of Nanoscience and Nanotechnology 7, 1804–1809
Soltanian S.; Horvat J.; L.Wang X.; Munroe P. & Dou S. X. (2003). Physica C, vol. 390, pp. 185–190
Thompson J. R.; Sun Y.; Christen D.; Civale L.; Marwick A. & Holtzberg F (1994). Phys. Rev. B 49, 13287; Thompson J. R.; Krusin Elbaum L.; Civale L.; Blatter G. & Field C. (1997). Phys. Rev. Lett. 78, 3181.
Ueda S.; Shimoyama J. I.; Yamamoto A.; Katsura Y.; Iwayama I.; Horii S. & Kishio K., (2005). Physica C, vol.426–431, pp. 1225–1230
Vajpayee A.; Awana V. P.S.; Yuc S.; Bhalla G.L. & Kishan H. (2010). Physica C 470 S653–S654
Wilke R. H. T.; Bud'ko S. L.; Candfield P. C.; Finnemore D. K.; Suplinskas R. J. & Hannahs S. T. (2004). Phys. Rev. Lett. 92, 217003-217007
Wilke R. H. T.; Bud'ko S. L.; Canfield P. C.; Finnemore D. K.; Suplinskas R. J. & Hannahs S. T. (2005a). Physica C 424, 1-16
Wilke R. H. T.; Bud'ko S. L.; Canfield P. C.; Finnemore D. K.; & Hannahs S T (2005b). Physica C 432, 193-205
Xu A.; Ma Y.; Wang D. L.; Gao Z. S.; Zhang X. P, & Watanabe K. (2007). Physica C, 466, 190-195
Yamamoto A.; Shimoyama J. I.; Ueda S.; Katsura Y.; Horii S. & Kishio K., (2005a). IEEE Trans. Appl. Supercond., vol. 15, pp. 3292–3295
Yamamoto A.; Shimoyama J. I.; Ueda S.; Iwayama I.; Horii S. & Kishio K. (2005b). Supercond. Sci. Technol., vol. 18, pp. 1323–1328
Yeoh W K.; Horvat J.; Dou S. X. & Keast V. (2004). Supercond. Sci. Technol. 17, S572
Yeoh W K.; Horvat J.; Dou S. X. & Munroe P. (2005). IEEE Trans Appl. Supercond. 15, 3284-3287

Yeoh W. K.; Kim J. H.; Horvat J.; Dou S. X. & Munroe P. (2006). Supercond. Sci. Technol. 19, L5-L8
Yeshurun Y.; Malozemoff A.P ; Shaulov A. (1996). Rev. Mod. Phys. 68, 911

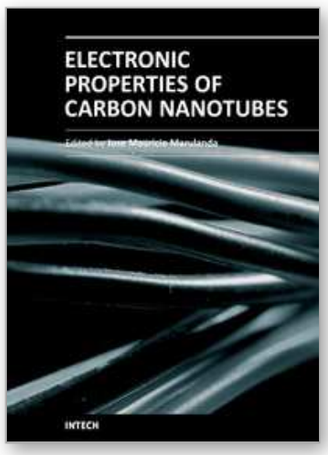

Electronic Properties of Carbon Nanotubes
Edited by Prof. Jose Mauricio Marulanda

ISBN 978-953-307-499-3
Hard cover, 680 pages
Publisher InTech
Published online 27, July, 2011
Published in print edition July, 2011

Carbon nanotubes (CNTs), discovered in 1991, have been a subject of intensive research for a wide range of applications. These one-dimensional (1D) graphene sheets rolled into a tubular form have been the target of many researchers around the world. This book concentrates on the semiconductor physics of carbon nanotubes, it brings unique insight into the phenomena encountered in the electronic structure when operating with carbon nanotubes. This book also presents to reader useful information on the fabrication and applications of these outstanding materials. The main objective of this book is to give in-depth understanding of the physics and electronic structure of carbon nanotubes. Readers of this book should have a strong background on physical electronics and semiconductor device physics. This book first discusses fabrication techniques followed by an analysis on the physical properties of carbon nanotubes, including density of states and electronic structures. Ultimately, the book pursues a significant amount of work in the industry applications of carbon nanotubes.

How to reference
In order to correctly reference this scholarly work, feel free to copy and paste the following:

Adriana Serquis, Gabriela Pasquini and Leonardo Civale (2011). Carbon Nanotubes Addition Effects on MgB2 Superconducting Properties, Electronic Properties of Carbon Nanotubes, Prof. Jose Mauricio Marulanda (Ed.), ISBN: 978-953-307-499-3, InTech, Available from: http://www.intechopen.com/books/electronic-properties-of-carbon-nanotubes/carbon-nanotubes-addition-effects-on-mgb2-superconducting-properties

INTECH
open science | open minds

InTech Europe
University Campus STeP Ri
Slavka Krautzeka 83/A
51000 Rijeka, Croatia
Phone: +385 (51) 770 447
Fax: +385 (51) 686 166
www.intechopen.com

InTech China
Unit 405, Office Block, Hotel Equatorial Shanghai
No.65, Yan An Road (West), Shanghai, 200040, China
中国上海市延安西路65号上海国际贵都大饭店办公楼405单元
Phone: +86-21-62489820
Fax: +86-21-62489821

IntechOpen